Staircase modulation improvement to balance output power of stages of cascade H-bridge multilevel inverter

Alireza Sedaghati, Pablo Horrillo-Quintero, Higinio Sánchez-Sainz, and Luis M. Fernández-Ramírez

Published in:
Computers and Electrical Engineering

DOI (link to publication from Publisher):
https://doi.org/10.1016/j.compeleceng.2022.108331

Publication date:
2022

Document Version:
Accepted version

Citation for published version:
Alireza Sedaghati, Pablo Horrillo-Quintero, Higino Sánchez-Sáinz, Luis M. Fernández-Ramírez,
Staircase modulation improvement to balance output power of stages of cascade H-bridge multilevel inverter,
Computers and Electrical Engineering,
Volume 103,
2022,
108331,
ISSN 0045-7906,
https://doi.org/10.1016/j.compeleceng.2022.108331.
(https://www.sciencedirect.com/science/article/pii/S0045790622005511)

Staircase modulation improvement to balance output power of stages of cascade H-bridge multilevel inverter

Alireza Sedaghati[1,*], Pablo Horrillo-Quintero[1], Higino Sánchez-Sáinz[2], Luis M. Fernández-Ramírez[1]

[1] *Research Group in Sustainable and Renewable Electrical Technologies (PAIDI-TEP023), Department of Electrical Engineering, Higher Technical School of Engineering of Algeciras (ETSIA), University of Cadiz,* Algeciras, Spain.

[2] *Research Group in Sustainable and Renewable Electrical Technologies (PAIDI-TEP023), Department of Electrical Engineering, High School of Engineering, University of Cadiz,* Puerto Real, Spain.

Abstract

In this study, different methods were investigated to minimize the power imbalance between the stages of a cascade H-bridge (CHB) multilevel inverter (MLI). First-in-first-out (FIFO) and first-in-last-out (FILO) are two common staircase-modulation (SCM) methods. A CHB-MLI with FIFO modulation, even with the same conduction times, cannot distribute power equally between the stages. A new algorithm is presented in this study to balance the power between the inverter stages. This is important to increase the lifetime of the PV sources that feed the inverter. To implement the new algorithm, all possible switching patterns based on the angles obtained from the nearest level of control (NLC) method are defined as the sample spaces of random variables. Subsequently, a random vector is defined for a set of random variables, and an optimization problem with finite and discrete solutions is applied. This algorithm is effectively used to minimize the power imbalance between the stages, even in impedance loads, from the purely inductive to the pure capacitive range. In addition, with slight changes in the switching angles, the operation of the stages and the inverter efficiency increases. Finally, the simulation and experimental results confirm the validity and practicality of the proposed modulation.

Keywords: Power balancing, cascade H-bridge multilevel inverter (CHB-MLI), staircase modulation (SCM), nearest level of control (NLC) utilization, total harmonic distortion (THD).

1. Introduction

* Corresponding author
E-mail addresses: eerfaculty@yahoo.com (A. Sedaghati), pablo.horrillo@uca.es (P. Quintero-Horrillo), higinio.sanchez@uca.es (H. Sanchez-Sainz), luis.fernandez@uca.es (L. M. Fernández-Ramírez)

Currently, MLIs have replaced two-level models in many applications. An MLI can produce an output voltage that is closer to sinusoidal, thereby reducing the need for expensive filtering [1]. Among the three different topologies of MLIs, CHB-MLI is the most widely used topology [2,3] and is based on several single-phase series connections of H-bridge cells. This structure can generate a high voltage on the output side using separate DC sources. This topology operates at high switching frequencies and produces an almost sinusoidal output waveform. CHB-MLIs were developed at three, five, and seven levels according to the structure and modulation methods [4,5]. Various modulation techniques have been proposed for CHB-MLI [6,7]. Sinusoidal pulse-width modulation (SPWM) with phase change (PC) and level change (LC) is the most popular high frequency modulations [8]. Low-frequency modulations such as SCM [9,10] are preferable to high-frequency modulations in terms of switching losses, and do not require expensive filters [11]. The problem with the SCM is that the output voltage cannot be increased or decreased over a wide range. However, this can be achieved using the SPWM.

The advantage of CHB-MLIs is that they operate at high voltages and power, and their disadvantages include unbalanced power distribution between the stages and the use of energy storage systems [12,13]. Inverters with photovoltaic (PV) sources are often used in the form of single-phase H-bridges to generate electricity. They are equipped with advanced methods for modulation or topology of inverters [14]. However, the output-power imbalance for different stages has not received significant attention. The lack of power balance between PV modules causes H-bridges to have more power losses. Some studies have reduced the power deviation between stages by improving SPWM [15,16]. In three-phase inverters, a power imbalance between the phases causes asymmetry in the network current [17]. However, the power imbalance between the stages causes unequal switching losses and different conduction times for each stage [18]. In [19], to balance the power between the phases and stages of a three-phase CHBMLI, DC voltage isolation was used by intermediate transformers in a DC-DC converter, which is expensive. Although intermediate transformers operate at high frequencies, the use of large capacitors is essential for eliminating these high frequencies. A hybrid method of high- and low-frequency modulation was implemented in [20], however, the problem was the existence of DC voltage fluctuations. In [21], power deviations between cells and between phases were investigated separately for a three-phase CHB-MLI connected to a grid with an unbalanced voltage. It was solved using a zero-sequence current source and structure presented in [22]. In [23], a method for balancing the power with strong damping of the transient response was proposed for a three-phase modular rectifier. In [24], CHBMLIs with high- and low-voltage

stages were considered, and hybrid modulation was applied for power balance between stages. A hybrid SPWM based on low-frequency modulation for high-voltage stages and high-frequency modulation for low-voltage stages was used in [25]. The power imbalances between the CHB-MLI modules were solved in [26] by changing the modulation carrier. A trapezoidal carrier was implemented instead of a triangular pulse, which helped reduce the power imbalance. However, some studies have used low-frequency modulation to reduce the power deviation between the inverter stages. In [27], a different turn ratio for a single-phase transformer-based CHB-MLI was used to approximate the balance power between the stages. The need for expensive and bulky filters, owing to the presence of a transformer, is a disadvantage of this method. However, the power imbalance problem in low-frequency modulation methods such as SCM for transformerless inverters, has rarely been considered [28]. The power imbalance in FILO using the angles obtained from the NLC [29] method is mostly observed in resistive loads. In contrast, the FIFO method is problematic for inductive or capacitive loads and has an almost uniform distribution for resistive loads. In [28], a method for achieving power balance between stages using the switching angles of each half-cycle was proposed. In this method, the calculations increase exponentially with an increase in the number of stages and start again by changing the load power factor.

In this study, a new algorithm called balanced power staircase modulation (BPSCM) is proposed to minimize the power deviation between the stages. This algorithm was developed based on the power analysis of inverter cells as the sample space of a random vector and can be implemented practically using simple calculations. Therefore, the main innovation of this study is the development of an algorithm to determine the switching pattern based on the SCM strategy, such that it can balance the power between the stages of CHB-MLIs as much as possible for impedance loads with different load angles. This static algorithm includes simple calculations that can be specified by the number of stages and does not depend on the load angle. The above algorithm, in the form presented in this article, has not been reported in the literature so far, and the existing methods based on low-frequency modulations include heavy and complex calculations with load dependence.

The remainder of this paper is organized as follows. First, the power equations of the inverter stages are studied using the existing SCM methods described in Section 2. Their strengths and weaknesses were examined and analyzed using a few examples. Based on this, BPSCM is developed in Section 3 as a finite and discrete optimization problem. An algorithm for its implementation is presented in Section 4. Section 5

presents a numerical analysis of the switching patterns for different stages. Some technical considerations are provided in Sections 5.1 and 5.2. Section 6 presents and discusses the results obtained from the simulation and the experimental setup. Both the results confirm the efficiency of the proposed method. Finally, section 7 presents the conclusions of this study.

2. Analysis of stages power balance by SCM

First, the power of each stage in the MLI is calculated. For simplicity, a 3-stage CHB-MLI connected to the impedance load is considered shown in Fig. 1(a). Fig. 1(b) shows the output voltage and current waveforms of the inverter, which is operated by FIFO modulation. The current waveforms of all stages and the inverter are the same. The output voltage is expressed as follows:

$$v(t) = v_{max}Sin(\theta), i(t) = i_{max}Sin(\theta + \varphi), \quad \theta = 2\pi f_0 t \tag{1}$$

Where f_0 is the main frequency, and φ is the load angle. It can be positive for a capacitive-resistive load, or negative for an inductive-resistive load.

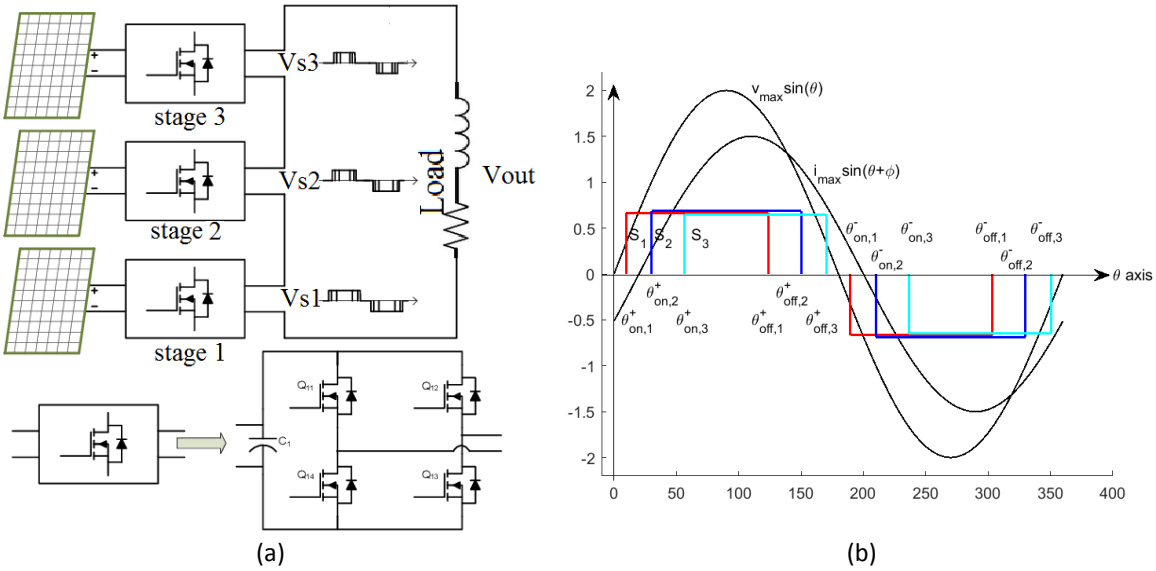

Fig. 1. A 3-stage CHB-MLI is fed by PV solar panels and operated by FIFO. (a) Schematic diagram. (b) Output voltage of stages, output voltage, and current of inverter connected to impedance load.

The switching angles include superscript + for the positive and - for the negative half-cycle. It is assumed that the average power is calculated for two half-cycles. This issue will be addressed in the following sections. Each angle in the positive and negative half-cycles includes "on" and "off" positions. For example, $\theta^{+}_{on,1}$ indicates the turn-on angle of the first stage in the positive half-cycle, and so on. It is assumed that the DC sources for all stages are equal to V_{DC}. The average power for k-th stage in Fig. 1, or P_{av,S_k} is:

$$P_{av,S_k} = \frac{1}{2\pi}\left\{\int_{\theta^+_{on,k}}^{\theta^+_{off,k}} V_{DC} i_{max} \sin(\theta+\varphi)\, d\theta - \int_{\theta^-_{on,k}}^{\theta^-_{off,k}} V_{DC} i_{max} \sin(\theta+\varphi)\, d\theta\right\} \quad (2)$$

where i_{max} is the maximum current of the impedance load $Z = R + jX$, which is equal to $v_{max}/|Z|$, where $|Z| = \sqrt{R^2 + X^2}$ and $\varphi = \tan^{-1} X/R$.

$$P_{av,S_k} = \frac{V_{DC} i_{max}}{2\pi}\cdot \begin{Bmatrix} \cos(\theta^+_{on,k}+\varphi) - \cos(\theta^+_{off,k}+\varphi) \dots \\ \dots - \cos(\theta^-_{on,k}+\varphi) + \cos(\theta^-_{off,k}+\varphi) \end{Bmatrix} \quad (3)$$

The factor $A = \frac{V_{DC} i_{max}}{2\pi}$ was set to 1. In this case, the stage power in (3) has a per-unit value. The turn-on angles in the positive half-cycle are:

$$Sin(\theta^+_{on,k}) = (k - 1 + \beta)\frac{V_{DC}}{v_{max}} \quad (4)$$

where β is a coefficient between 0 and 1 [11]. If $\beta = 0.5$, the angles obtained from (4) are the same as those obtained using the NLC method [30]. The modification of β is discussed in the following sections. It can be assumed that $\frac{V_{DC}}{v_{max}} = \frac{1}{N}$ for N stages, and v_{max} is the output voltage.

2.1. Calculating the output power of each stage

The turn-on angles in the positive half-cycle for the 3-stage inverter in Fig. 1 are obtained using (4) as follows:

$$\theta^+_{on,1} = \sin^{-1}\left(\frac{1}{2}\frac{1}{3}\right) = 9.5941^o\,,\ \theta^+_{on,2} = \sin^{-1}\left(\frac{3}{2}\frac{1}{3}\right) = 30.0^o$$
$$\theta^+_{on,3} = \sin^{-1}\left(\frac{5}{2}\frac{1}{3}\right) = 56.4427^o \quad (5)$$

For the FIFO method, the turn-off angles in the positive half-cycle and the turn-on and turn-off angles in the negative half-cycle can be calculated as follows:

$$\theta^+_{off,1} = \pi - \theta^+_{on,3}\,,\theta^+_{off,2} = \pi - \theta^+_{on,2}\,,\theta^+_{off,3} = \pi - \theta^+_{on,1}$$
$$\theta^-_{off,1} = 2\pi - \theta^+_{on,3}\,,\theta^-_{off,2} = 2\pi - \theta^+_{on,2}\,,\ \ \theta^-_{off,3} = 2\pi - \theta^+_{on,1}$$
$$\theta^-_{on,1} = \pi + \theta^+_{on,1}\,,\qquad \theta^-_{on,2} = \pi + \theta^+_{on,2}\,,\theta^-_{on,3} = \pi + \theta^+_{on,3} \quad (6)$$

Therefore, the per-unit power of each stage is equal to:

$$
\begin{aligned}
P_{av,S_1} &= \left\{ \begin{matrix} \cos\left(\theta_{on,1}^{+} + \varphi\right) + \cos\left(\theta_{on,3}^{+} - \varphi\right) \\ +\cos\left(\theta_{on,1}^{+} + \varphi\right) + \cos\left(\theta_{on,3}^{+} - \varphi\right) \end{matrix} \right\} \\
P_{av,S_2} &= \left\{ \begin{matrix} \cos\left(\theta_{on,2}^{+} + \varphi\right) + \cos\left(\theta_{on,2}^{+} - \varphi\right) \\ +\cos\left(\theta_{on,2}^{+} + \varphi\right) + \cos\left(\theta_{on,2}^{+} - \varphi\right) \end{matrix} \right\} \\
P_{av,S_3} &= \left\{ \begin{matrix} \cos\left(\theta_{on,3}^{+} + \varphi\right) + \cos\left(\theta_{on,1}^{+} - \varphi\right) \\ +\cos\left(\theta_{on,3}^{+} + \varphi\right) + \cos\left(\theta_{on,1}^{+} - \varphi\right) \end{matrix} \right\}
\end{aligned} \tag{7}
$$

The power of stages for resistive load or $\varphi = 0$ are as follows:

$$
\begin{aligned}
P_{av,S_1}\big|_{\varphi=0} = P_{av,S_3}\big|_{\varphi=0} &= 2\{\cos\left(\theta_{on,1}^{+}\right) + \cos\left(\theta_{on,3}^{+}\right)\}=3.0776 \\
P_{av,S_2}\big|_{\varphi=0} &= 2\{\cos\left(\theta_{on,2}^{+}\right) + \cos\left(\theta_{on,2}^{+}\right)\}=3.4641
\end{aligned} \tag{8}
$$

The power of stages for a pure capacitive or inductive load, or $\varphi = \pm 90$ obtained from (4), is equal to:

$$
\begin{aligned}
P_{av,S_1}\big|_{\varphi=\pm 90} &= -2sin\left(\theta_{on,1}^{+}\right) + 2\sin\left(\theta_{on,3}^{+}\right) = \pm 4/3 \\
P_{av,S_2}\big|_{\varphi=0} &= -2sin\left(\theta_{on,2}^{+}\right) + 2\sin\left(\theta_{on,2}^{+}\right) = 0 \\
P_{av,S_3}\big|_{\varphi=\pm 90} &= +2sin\left(\theta_{on,1}^{+}\right) - 2\sin\left(\theta_{on,3}^{+}\right) = \mp 4/3
\end{aligned} \tag{9}
$$

The power of stages in the FIFO for the resistive load is close to each other. However, for purely inductive or capacitive loads, they are completely different, although the conduction time of each stage is the same. It is shown by the dashed lines in Fig. 2. For the FILO, the following can be written:

$$
\begin{aligned}
\theta_{off,1}^{+} = \pi - \theta_{on,1}^{+}\,, \theta_{off,1}^{-} = 2\pi - \theta_{on,1}^{+} \\
\theta_{off,2}^{+} = \pi - \theta_{on,2}^{+}\,, \theta_{off,2}^{-} = 2\pi - \theta_{on,2}^{+} \\
\theta_{off,3}^{+} = \pi - \theta_{on,3}^{+}\,, \theta_{off,3}^{-} = 2\pi - \theta_{on,3}^{+} \\
\theta_{on,1}^{-} = \pi + \theta_{on,1}^{+}\,, \theta_{on,2}^{-} = \pi + \theta_{on,2}^{+}\,, \theta_{on,3}^{-} = \pi + \theta_{on,3}^{+}
\end{aligned} \tag{10}
$$

The power of stages is obtained using (4) for two load angles of $\varphi = 0$ and $\varphi = \pm 9$ as follows:

$$
\begin{aligned}
P_{av,S_1}\big|_{\varphi=0} = 2\{2\cos\left(\theta_{on,1}^{+}\right)\}=3.9441,\ P_{av,S_2}\big|_{\varphi=0} &= 2\{2\cos\left(\theta_{on,2}^{+}\right)\}=3.4641 \\
P_{av,S_3}\big|_{\varphi=0} &= 2\{2\cos\left(\theta_{on,3}^{+}\right)\}=2.2111 \\
P_{av,S_1}\big|_{\varphi=\pm 90} = P_{av,S_2}\big|_{\varphi=\pm 90} &= P_{av,S_3}\big|_{\varphi=\pm 90} = 0
\end{aligned} \tag{11}
$$

As indicated by the solid line in Fig. 2, the FILO method has the highest power deviation between the stages for resistive loads, and zero power deviation for inductive or capacitive loads. The algorithm in [28] includes complex calculations and depends on the load angle, which is difficult to implement practically. Each time the load angle changes, the switching pattern must be recalculated. The hardware required to implement this algorithm is complex, and thus, its calculations take approximately 7 hours for a 7-level

inverter with a 1.2 GHz processor, which can be easily replaced by rotating the switching angles in different cycles.

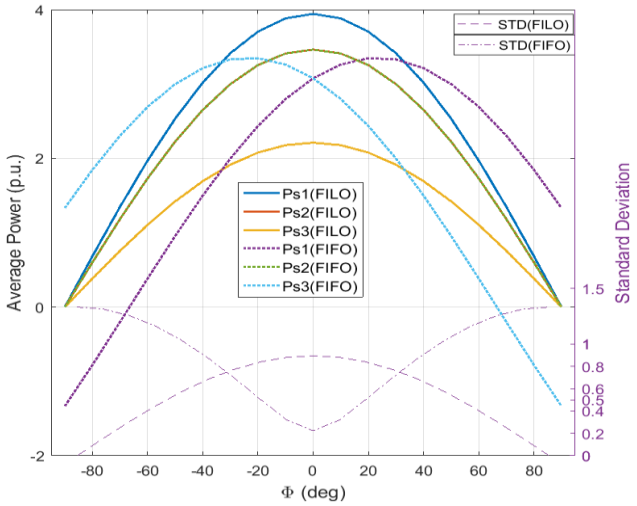

Fig. 2. Average power of stages for the 3-level inverter, with FIFO in dash line and FILO in solid line. The standard deviation of the two methods are also indicated on the right-hand axis.

2.2. Analysis of the least deviation of stages power

As shown in Fig. 2, it is desirable to find an algorithm that works like FIFO for resistive loads, and FILO for inductive/capacitive loads. Because the average power is calculated in two half-cycles, as shown in (2), the power of each stage includes two cosine terms. An inverter with N stages has N turn-on angles during the first half cycle. Therefore, a pair of N angles should be selected, such that the sum of their cosines is approximately equal. Consequently, the sum of the cosine of the angles can be attributed to a random variable with a sample space of 2 combinations of N. For example, in a 3-stage inverter, 2 permutations of 3 cosine terms, including $\cos(\theta^{+}_{on,1})$, $\cos(\theta^{+}_{on,2})$, and $\cos(\theta^{+}_{on,3})$ are considered as the sample space of the random variable $\boldsymbol{P}$, which consists of 6 terms as follows:

$$\boldsymbol{P} = \begin{Bmatrix} \cos(\theta^{+}_{on,1}) + \cos(\theta^{+}_{on,1}), \\ \cos(\theta^{+}_{on,1}) + \cos(\theta^{+}_{on,2}), \\ \cos(\theta^{+}_{on,1}) + \cos(\theta^{+}_{on,3}), \\ \cos(\theta^{+}_{on,2}) + \cos(\theta^{+}_{on,2}), \\ \cos(\theta^{+}_{on,2}) + \cos(\theta^{+}_{on,3}), \\ \cos(\theta^{+}_{on,3}) + \cos(\theta^{+}_{on,3}) \end{Bmatrix} = \begin{Bmatrix} 1.9732, \\ 1.8526, \\ 1.5394, \\ 1.7320, \\ 1.4188, \\ 1.1056 \end{Bmatrix} \quad (12)$$

The mean of $\boldsymbol{P}$ is equal to 1.6036. The absolute value of the standard deviation of the third element is lower than those of the other elements. The lowest deviation belongs to the fourth element. Because the angles obtained from (4) are ascending, their cosines are descending, and the sum of $\cos(\theta^{+}_{on,1}) +$

$\cos(\theta^+_{on,3})$ is closer to the sum of $\cos(\theta^+_{on,2}) + \cos(\theta^+_{on,2})$. For example, for a 4-stage inverter, the sum of $\cos(\theta^+_{on,1}) + \cos(\theta^+_{on,4})$ should be closer to the sum of $\cos(\theta^+_{on,2}) + \cos(\theta^+_{on,3})$ than the other options. In general, a selection 2 of N cosine terms that are closest to each other can be described as follows:

$$\begin{aligned}\cos(\theta^+_{on,1}) + \cos(\theta^+_{on,N}) \approx \cos(\theta^+_{on,2}) + \cos(\theta^+_{on,N-1}) \approx \cdots \\ \approx \begin{cases} 2\cos(\theta^+_{on,N+1/2}) \; for\; N\; is\; odd \\ \cos(\theta^+_{on,N/2}) + \cos\left(\theta^+_{on,\frac{N}{2}+1}\right) \; for\; N\; is\; even \end{cases}\end{aligned} \tag{13}$$

Note that this rule is not approximate for the sum of the sine terms of the first quadrant angles owing to (4) but is exactly equal. That is, the sum of $\sin(\theta^+_{on,1}) + sin(\theta^+_{on,3})$ is equal to the sum of $\sin(\theta^+_{on,2}) + sin(\theta^+_{on,2})$ or, in general, due to (4), the following is true:

$$\begin{aligned}\sin(\theta^+_{on,1}) + sin(\theta^+_{on,N}) = sin(\theta^+_{on,2}) + sin(\theta^+_{on,N-1}) = \cdots \\ = \begin{cases} 2\sin(\theta^+_{on,N+1/2}) \; for\; N\; is\; odd \\ \sin(\theta^+_{on,N/2}) + sin\left(\theta^+_{on,\frac{N}{2}+1}\right) \; for\; N\; is\; even \end{cases}\end{aligned} \tag{14}$$

Therefore, Eq. (8) provides the optimum switching pattern for a 3-stages inverter with φ=0. From circuit analysis, the power of inductive or capacitive loads is zero; however, the power of each stage may be positive or negative. Consequently, some stages can consume power, which causes technical problems. Therefore, the next goal of this study is to determine an algorithm similar to FIFO, in which the power of each stage should be zero for net impedance loads. For this purpose, an optimization problem with finite and discrete solutions and circuit constraints must be solved, as explained in the next section. From the solution of this optimization problem, it is concluded that the power deviation of the stages has a maximum value for the load angle φ=0. In other words, the power deviation between stages is smaller for φ≠0. Therefore, the focus of the algorithm design is to minimize the power deviation for the load with φ=0, and complex calculations are no longer required for each change in φ.

3. Optimization problem to balance power of stages

The discrete and finite solutions of the following optimization problem subject to the corresponding constraints provide an optimal switching pattern that balances the power between the stages.

$$\begin{aligned}&\min\left\{max_{\Phi}\{\sigma^2(\boldsymbol{P}_{av,S}, \Theta, \Phi)\}\right\} \\ &\text{subject to: } \sigma^2(\boldsymbol{P}_{av,S}, \Theta, \pm\pi/2) = 0\end{aligned} \tag{15}$$

where Φ is a random variable with a sample space of discrete intervals from $-\pi/2$ to $+\pi/2$ in steps of $\Delta\Phi$ degree. The random variable of stage S includes the sample spaces s_1 to s_N.

$$\Phi = \{[-\pi/2, +\pi/2]\}\,,\ \Theta = \{\theta^{+}_{on,1}, \theta^{+}_{on,2}, \dots, \theta^{+}_{on,N}\}\,,\ S = \{s_1, s_2, \dots, s_N\} \tag{16}$$

The turn-on and off angles of each stage are determined for two positive and negative half-cycles. Therefore, the output power of each stage can be defined by using the following random variable:

$$\boldsymbol{P}_{av,S} = \cos(\Theta + \Phi) - \cos(\pi - \Theta + \Phi) - \cos(\pi + \Theta + \Phi) + \cos(2\pi - \Theta + \Phi) \tag{17}$$

In general, the sample space of the random variable $\boldsymbol{P}_{av,S_k}$ for N stages contains N! terms. Therefore, the random vector $\boldsymbol{P}_{av,S}$ including the average power random variables, has a sample space with dimensions of $(\boldsymbol{N}!)^{\boldsymbol{N}}$. A fixed algorithm can be found for the optimal solution of (15), although it is not unique. The standard deviation of the random vector $\boldsymbol{P}_{av,S}$ reaches its maximum value at $\varphi = 0$, due to the power constraints of (15). Therefore, it is sufficient to minimize the standard deviation of the switching pattern for $\varphi = 0$. The solution of (15) is obtained for a 3-stage inverter as follows.

3.1. Solution for a 3-stage inverter

This section presents the solution to the optimization problem defined in (15) for a 3-stage inverter. Suppose that the turn-on angles in the positive half-cycle for each stage are determined by using (4). For simplicity, suppose that $\varphi = 0$. The number of sample spaces of the power random variable for the first stage is given by:

$$\boldsymbol{P}_{av,S_1} = \cos\left(\theta^{+}_{on,1}\right) + \begin{Bmatrix}\cos\left(\theta^{+}_{on,1}\right)\\ \cos\left(\theta^{+}_{on,2}\right)\\ \cos\left(\theta^{+}_{on,3}\right)\end{Bmatrix} + \begin{Bmatrix}\cos\left(\theta^{+}_{on,1}\right)\\ \cos\left(\theta^{+}_{on,2}\right)\\ \cos\left(\theta^{+}_{on,3}\right)\end{Bmatrix} + \begin{Bmatrix}\cos\left(\theta^{+}_{on,1}\right)\\ \cos\left(\theta^{+}_{on,2}\right)\\ \cos\left(\theta^{+}_{on,3}\right)\end{Bmatrix} \tag{18}$$

For each clause, there are 3!=6 modes, and for each stage, there are $(6)^3 = 218$ cases. By implementing the optimization problem with the limited and discrete solutions of (15) for a 3-stage inverter, the optimal solution can be obtained as follows:

$$\begin{aligned} P_{av,S_1} &= \begin{Bmatrix}\cos\left(\theta^{+}_{on,1} + \varphi\right) + \cos\left(\theta^{+}_{on,2} - \varphi\right)\\ +\cos\left(\theta^{+}_{on,3} + \varphi\right) + \cos\left(\theta^{+}_{on,2} - \varphi\right)\end{Bmatrix}\\ P_{av,S_2} &= \begin{Bmatrix}\cos\left(\theta^{+}_{on,2} + \varphi\right) + \cos\left(\theta^{+}_{on,2} - \varphi\right)\\ +\cos\left(\theta^{+}_{on,2} + \varphi\right) + \cos\left(\theta^{+}_{on,2} - \varphi\right)\end{Bmatrix}\\ P_{av,S_3} &= \begin{Bmatrix}\cos\left(\theta^{+}_{on,3} + \varphi\right) + \cos\left(\theta^{+}_{on,2} - \varphi\right)\\ +\cos\left(\theta^{+}_{on,1} + \varphi\right) + \cos\left(\theta^{+}_{on,2} - \varphi\right)\end{Bmatrix} \end{aligned} \tag{19}$$

By calculating the output power of the three stages for $\varphi = 0$, the following expression is obtained:

$$P_{av,S_1}\big|_{\varphi=0} = P_{av,S_3}\big|_{\varphi=0} = \cos\left(\theta^{+}_{on,1}\right) + \cos\left(\theta^{+}_{on,3}\right) + 2\cos\left(\theta^{+}_{on,2}\right)$$
$$P_{av,S_2}\big|_{\varphi=0} = 2\cos\left(\theta^{+}_{on,2}\right) + 2\cos\left(\theta^{+}_{on,2}\right) \quad (20)$$

The powers of the first and third stages are the same and exhibited the least deviation from the power of the second stage. From (4), for $\varphi = \pm 90$ the following can be derived:

$$P_{av,S_1}\big|_{\varphi=\pm 90} = P_{av,S_3}\big|_{\varphi=\pm 90} = \mp sin\left(\theta^{+}_{on,1}\right) \pm 2\sin\left(\theta^{+}_{on,2}\right) \mp sin\left(\theta^{+}_{on,3}\right) = 0$$
$$P_{av,S_2}\big|_{\varphi=\pm 90} = \mp 2sin\left(\theta^{+}_{on,2}\right) \pm 2\sin\left(\theta^{+}_{on,2}\right) = 0 \quad (21)$$

Based on the optimal solution of (15) and the above calculations, an algorithm is presented in the next section. With the new algorithm, there is no need to repeat the calculations for every change in φ because the maximum power deviation occurs at φ=0.

4. Optimal switching pattern algorithm to minimize the power deviation between stages

To determine the desired algorithm, consider the average power of each stage in two positive and negative half-cycles, which includes the sum of the four cosine terms of the angles, given by (4). As the number of half-cycles required to calculate the average power increases, the number of cosine terms also increased by the same amount. The optimal solution (15) is similar to solving the Sudoku table with the following characteristics: the table contains four columns, and the number of rows is equal to the number of the inverter stages N. It is assumed that each stage is turned on at the angle of the first quarter given by (4). From (13), it is concluded that for the smallest power deviation, there must be a cosine term of the angle of stage N-k corresponding to the cosine term of the angle of stage k. Therefore, in the third column, the angles of the first column are placed in the ascending order of the stage index, as shown in Table I. the coefficient γ is equal to 0 for an even number and 1 for an odd number of N stages.

For$\varphi = \pm 90$, the first and third columns contain negative sine angles, and the second and fourth columns contain positive sine angles. Therefore, columns 1 and 3 are completed first so that both the power deviations of these two columns are minimal. Then, for $\varphi = \pm 90$, the sum of the negative and positive sine terms that are placed in columns 2 and 4 must be equal to zero. Thus far, the sum of the powers of each stage has exhibited the least deviation. The table is Sudoku-like because in each column, all angles in (4) should exist, and none of them should be repeated. There should also be 2 combinations of N angles in each row, as in (13), that have the least power deviation. For example, in row 1 of columns

2 and 4, there can be any combination such as $(\theta^{+}_{on,2}, \theta^{+}_{on,N-1})$, $(\theta^{+}_{on,3}, \theta^{+}_{on,N-2})$, etc. Although the table has several solutions with the feature of the least power deviation, to determine a fixed formula for preparing the table by considering constraints (14), the following algorithm is proposed to fill out columns 2 and 4 as shown in the flow chart in Fig. 3.

Table I. Switching pattern for balancing the power of stages. $\gamma = 1$ for N is odd and $\gamma = 0$ for N is even.

Stage #	θ^{+}_{on}	$\pi - \theta^{+}_{off}$	$\theta^{-}_{on} - \pi$	$2\pi - \theta^{-}_{off}$
S_1	$\theta^{+}_{on,1}$	$\theta^{+}_{on,(N-\gamma)/2}$	$\theta^{+}_{on,N}$	$\theta^{+}_{on,(N+2+\gamma)/2}$
S_2	$\theta^{+}_{on,2}$	$\theta^{+}_{on,(N-2-\gamma)/2}$	$\theta^{+}_{on,N-1}$	$\theta^{+}_{on,(N+4+\gamma)/2}$
…	…	…	…	…
$S_{(N-\gamma)/2}$	$\theta^{+}_{on,(N-\gamma)/2}$	$\theta^{+}_{on,1}$	$\theta^{+}_{on,(N+2+\gamma)/2}$	$\theta^{+}_{on,N}$
…	…	…	…	…
S_{N-1}	$\theta^{+}_{on,N-1}$	$\theta^{+}_{on,(N+4-\gamma)/2}$	$\theta^{+}_{on,2}$	$\theta^{+}_{on,(N-2+\gamma)/2}$
S_N	$\theta^{+}_{on,N}$	$\theta^{+}_{on,(N+2-\gamma)/2}$	$\theta^{+}_{on,1}$	$\theta^{+}_{on,(N+\gamma)/2}$

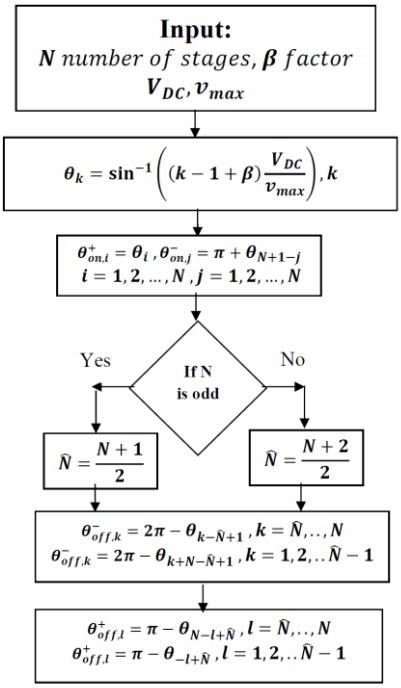

Fig. 3. Flowchart of the optimal switching pattern implemented in this study.

In the second column, if N is odd, the angles from index 1 to index (N-1)/2 are in row (N-1)/2 to row 1, and the angles from index (N+1)/2 to index N are in row N to row (N+1)/2. The second column, for even N, is similar to the case of odd N, except that the angle with index 1 is in the row N/2. The angles from index 1 to index N/2 are located in row N/2 to row 1, and the angles from index (N/2)+1 to index N are located in row N to row (N/2)+1. The two modes of N are integrated using the γ coefficient, as listed in Table I. The fourth column should be completed such that the sum of the angle indices of columns 1 and 3 is equal to the sum of the angle indices of columns 2 and 4, so that the power condition is zero at $\varphi = \pm 90$.

5. *Numerical analysis of switching patterns for different stages*

In this section, the algorithm shown in Fig. 3 is calculated for different numbers of inverter stages. Technical considerations were considered to further improve the solution. The efficiency of the BPSCM is also demonstrated by comparing the FIFO and FILO methods and calculating the maximum power deviation for $\varphi = 0$, where the power imbalance with the BPSCM method is proved to be maximum. The optimal switching patterns obtained by BPSCM for inverters with three, four, five, six, and seven stages are shown in Tables II–VI, respectively. The standard deviation of the power between the stages by the BPSCM is significantly lower than that of the two conventional methods. The values in the above tables are all calculated for $\beta = 0.5$ or the same as the usual NLC angles. The FILO exhibited the lowest power deviation for $\varphi = 0$, whereas BPSCM exhibited a smaller deviation. In contrast, FIFO has a power deviation of zero for $\varphi = \pm 90$, which is the same for the BPSCM algorithm because it was an essential constraint in the optimization problem of (15). This means that the optimal solution is based on the idea that in pure non-ohmic loads, the power deviation must be zero. Because all three methods create the same voltage waveform at the output, the THD of the output voltage is the same, and it decreases with an increase in the stages, as shown in the relevant tables.

Table II. Optimum switching pattern for N=3 and comparison of BPSCM with FILO and FIFO for $\beta = 0.5$

THD of output Voltage= 12.68%					Output power at $\varphi = 0$		
Stage#	θ_{on}^{+}	$\pi - \theta_{off}^{+}$	$\theta_{on}^{-} - \pi$	$2\pi - \theta_{off}^{-}$	FIFO	FILO	BPSCM
S_1	$\theta_{on,1}^{+}$	$\theta_{on,2}^{+}$	$\theta_{on,3}^{+}$	$\theta_{on,2}^{+}$	P=3.0776	3.9441	3.2708
S_2	$\theta_{on,2}^{+}$	$\theta_{on,1}^{+}$	$\theta_{on,2}^{+}$	$\theta_{on,3}^{+}$	3.4641	3.4641	3.2708
S_3	$\theta_{on,3}^{+}$	$\theta_{on,3}^{+}$	$\theta_{on,1}^{+}$	$\theta_{on,1}^{+}$	3.0776	2.2111	3.0776

Max $\sigma^2(P)$	1.3333	0.8948	0.1116

Table III. Optimum switching pattern for N=4 and comparison of BPSCM with FILO and FIFO for $\beta = 0.5$

THD of output Voltage= 9.89%					Output power at $\varphi = 0$		
Stage#	θ_{on}^{+}	$\pi - \theta_{off}^{+}$	$\theta_{on}^{-} - \pi$	$2\pi - \theta_{off}^{-}$	FIFO	FILO	BPSCM
S_1	$\theta_{on,1}^{+}$	$\theta_{on,2}^{+}$	$\theta_{on,4}^{+}$	$\theta_{on,3}^{+}$	2.9526	3.9686	3.1839
S_2	$\theta_{on,2}^{+}$	$\theta_{on,1}^{+}$	$\theta_{on,3}^{+}$	$\theta_{on,4}^{+}$	3.4153	3.7081	3.1839
S_3	$\theta_{on,3}^{+}$	$\theta_{on,4}^{+}$	$\theta_{on,2}^{+}$	$\theta_{on,1}^{+}$	3.4153	3.1225	3.1839
S_4	$\theta_{on,4}^{+}$	$\theta_{on,3}^{+}$	$\theta_{on,1}^{+}$	$\theta_{on,2}^{+}$	2.9526	1.9365	3.1839
Max $\sigma^2(P)$					1.2910	0.9038	0

Table IV. Optimum switching pattern for N=5 and comparison of BPSCM with FILO and FIFO for $\beta = 0.5$

THD of output Voltage= 8.23%					Output power at $\varphi = 0$		
Stage#	θ_{on}^{+}	$\pi - \theta_{off}^{+}$	$\theta_{on}^{-} - \pi$	$2\pi - \theta_{off}^{-}$	FIFO	FILO	BPSCM
S_1	$\theta_{on,1}^{+}$	$\theta_{on,3}^{+}$	$\theta_{on,5}^{+}$	$\theta_{on,3}^{+}$	2.8618	3.9799	3.0990
S_2	$\theta_{on,2}^{+}$	$\theta_{on,2}^{+}$	$\theta_{on,4}^{+}$	$\theta_{on,4}^{+}$	3.3362	3.8158	3.3362
S_3	$\theta_{on,3}^{+}$	$\theta_{on,1}^{+}$	$\theta_{on,3}^{+}$	$\theta_{on,5}^{+}$	3.4641	3.4641	3.1629
S_4	$\theta_{on,4}^{+}$	$\theta_{on,5}^{+}$	$\theta_{on,2}^{+}$	$\theta_{on,1}^{+}$	3.3362	2.8566	3.0990
S_5	$\theta_{on,5}^{+}$	$\theta_{on,4}^{+}$	$\theta_{on,1}^{+}$	$\theta_{on,2}^{+}$	2.8618	1.7436	3.1629
Max $\sigma^2(P)$					1.2649	0.9073	0.0972

Table V. Optimum switching pattern for N=6 and comparison of BPSCM with FILO and FIFO for $\beta = 0.5$

THD of output Voltage= 7.11%					Output power at $\varphi = 0$		
Stage#	θ_{on}^{+}	$\pi - \theta_{off}^{+}$	$\theta_{on}^{-} - \pi$	$2\pi - \theta_{off}^{-}$	FIFO	FILO	BPSCM
S_1	$\theta_{on,1}^{+}$	$\theta_{on,3}^{+}$	$\theta_{on,6}^{+}$	$\theta_{on,4}^{+}$	2.7923	3.9861	3.1175
S_2	$\theta_{on,2}^{+}$	$\theta_{on,2}^{+}$	$\theta_{on,5}^{+}$	$\theta_{on,5}^{+}$	3.2594	3.8730	3.2594
S_3	$\theta_{on,3}^{+}$	$\theta_{on,1}^{+}$	$\theta_{on,4}^{+}$	$\theta_{on,6}^{+}$	3.4426	3.6362	3.1175
S_4	$\theta_{on,4}^{+}$	$\theta_{on,6}^{+}$	$\theta_{on,3}^{+}$	$\theta_{on,1}^{+}$	3.4426	3.2489	3.1175
S_5	$\theta_{on,5}^{+}$	$\theta_{on,5}^{+}$	$\theta_{on,2}^{+}$	$\theta_{on,2}^{+}$	3.2594	2.6458	3.2594
S_6	$\theta_{on,6}^{+}$	$\theta_{on,4}^{+}$	$\theta_{on,1}^{+}$	$\theta_{on,3}^{+}$	2.7923	1.5986	3.1175
Max $\sigma^2(P)$					1.2472	0.9086	0.0733

Table VI. Optimum switching pattern for N=7 and comparison of BPSCM with FILO and FIFO for $\beta = 0.5$

THD of output Voltage= 6.35%					Output power at $\varphi = 0$		
Stage#	θ_{on}^{+}	$\pi - \theta_{off}^{+}$	$\theta_{on}^{-} - \pi$	$2\pi - \theta_{off}^{-}$	FIFO	FILO	BPSCM
S_1	$\theta_{on,1}^{+}$	$\theta_{on,3}^{+}$	$\theta_{on,7}^{+}$	$\theta_{on,5}^{+}$	2.7372	3.9898	3.0686
S_2	$\theta_{on,2}^{+}$	$\theta_{on,2}^{+}$	$\theta_{on,6}^{+}$	$\theta_{on,6}^{+}$	3.1907	3.9071	3.1907
S_3	$\theta_{on,3}^{+}$	$\theta_{on,1}^{+}$	$\theta_{on,5}^{+}$	$\theta_{on,7}^{+}$	3.4001	3.7362	3.0686
S_4	$\theta_{on,4}^{+}$	$\theta_{on,7}^{+}$	$\theta_{on,4}^{+}$	$\theta_{on,1}^{+}$	3.4641	3.4641	3.1007
S_5	$\theta_{on,5}^{+}$	$\theta_{on,6}^{+}$	$\theta_{on,3}^{+}$	$\theta_{on,2}^{+}$	3.4001	3.0639	3.2954
S_6	$\theta_{on,6}^{+}$	$\theta_{on,5}^{+}$	$\theta_{on,2}^{+}$	$\theta_{on,3}^{+}$	3.1907	2.4744	3.2954
S_7	$\theta_{on,7}^{+}$	$\theta_{on,4}^{+}$	$\theta_{on,1}^{+}$	$\theta_{on,4}^{+}$	2.7372	1.4846	3.1007
Max $\sigma^2(P)$					1.2344	0.9090	0.1011

5.1. Algorithm correction for even number of stages

Table IV lists the optimal switching patterns for N=4. On the one hand, the average power is calculated in two half-cycles, which includes four turn-on and off angles for each stage, and on the other hand, the number of stages is equal to 4. Therefore, the power of the four stages in the two half-cycles is the same, and the power deviation is zero. It is concluded that, if the number of stages is even, because each half cycle consists of two on/off angles, the average power calculation and the following switching pattern can be extended to the N/2 cycles. In this form, the average power of each stage has cosine terms for all angles, and the power deviation is zero. For example, for N=6, three half cycles can be used, and the switching pattern is shown in Table VII, where the superscript *k* for the turn-on and off angles indicates the angle in the k-th cycle, and $\theta_{on,1}^{+}$ to $\theta_{on,6}^{+}$ are obtained by (4) for N=6. In other words, the switching pattern in these three half-cycles is rotated for each stage [11].

Table VII. Optimum switching pattern for N=6, $\beta = 0.5$ by averaging power in three half cycles

Stage Number	θ_{on}^{1}	$\pi - \theta_{off}^{1}$	$\theta_{on}^{2} - \pi$	$2\pi - \theta_{off}^{2}$	$\theta_{on}^{3} - 2\pi$	$3\pi - \theta_{off}^{3}$
S_1	$\theta_{on,1}^{+}$	$\theta_{on,2}^{+}$	$\theta_{on,3}^{+}$	$\theta_{on,4}^{+}$	$\theta_{on,5}^{+}$	$\theta_{on,6}^{+}$
S_2	$\theta_{on,2}^{+}$	$\theta_{on,3}^{+}$	$\theta_{on,4}^{+}$	$\theta_{on,5}^{+}$	$\theta_{on,6}^{+}$	$\theta_{on,1}^{+}$
S_3	$\theta_{on,3}^{+}$	$\theta_{on,4}^{+}$	$\theta_{on,5}^{+}$	$\theta_{on,6}^{+}$	$\theta_{on,1}^{+}$	$\theta_{on,2}^{+}$
S_4	$\theta_{on,4}^{+}$	$\theta_{on,5}^{+}$	$\theta_{on,6}^{+}$	$\theta_{on,1}^{+}$	$\theta_{on,2}^{+}$	$\theta_{on,3}^{+}$
S_5	$\theta_{on,5}^{+}$	$\theta_{on,6}^{+}$	$\theta_{on,1}^{+}$	$\theta_{on,2}^{+}$	$\theta_{on,3}^{+}$	$\theta_{on,4}^{+}$
S_6	$\theta_{on,6}^{+}$	$\theta_{on,1}^{+}$	$\theta_{on,2}^{+}$	$\theta_{on,3}^{+}$	$\theta_{on,4}^{+}$	$\theta_{on,5}^{+}$

5.2. β factor correction

It is shown that the THD depends on β coefficient, and the best value of β which has the least harmonics on the output voltage, is 0.25 [11]. If the turn-on angles by (4) in the first quarter are calculated for β=0.25, it not only decreases the harmonics, but also the output power of each stage of the multilevel inverter has increased in comparison with the angles of $\beta = 0.5$ for the same DC sources. As shown in Table VIII, the output efficiency of the MLI increased. Furthermore, the power deviation between the stages is less than that in the case of $\beta = 0.5$. For $\beta = 0.75$ the power deviation is greater than that for $\beta = 0.5$.

Table VIII. Comparison of the output power and power deviation between stages for different β and levels using the BPSCM method

Power of stages for $\varphi = 0$	N=3		N=4		N=5		N=6		N=7	
	$\beta = 0.5$	$\beta = 0.25$	$\beta = 0.5$	$\beta = 0.25$	$\beta = 0.5$	$\beta = 0.25$	$\beta = 0.5$	$\beta = 0.25$	$\beta = 0.5$	$\beta = 0.25$
P_{S_1}	3.2708	3.4761	3.1839	3.3577	3.1629	3.3116	3.1175	3.2509	3.0686	3.1912
P_{S_2}	3.2708	3.4761	3.1839	3.3577	3.3362	3.4564	3.2594	3.3679	3.1907	3.2907
P_{S_3}	3.0776	3.3159	3.1839	3.3577	3.1629	3.3116	3.1175	3.2509	3.0686	3.1912
P_{S_4}			3.1839	3.3577	3.0990	3.2537	3.1175	3.2509	3.1007	3.2211
P_{S_5}					3.0990	3.2537	3.2594	3.3679	3.2954	3.3869
P_{S_6}							3.1175	3.2509	3.2954	3.3869
P_{S_7}									3.1007	3.2211
Total Powers	9.6192	10.2681	12.7357	13.4309	15.8599	16.5870	18.9886	19.7392	22.1201	22.8891
Max $\sigma^2(P)$	0.1116	0.0925	0	0	0.0972	0.0829	0.0733	0.0604	0.1011	0.0866
THD of V	12.68%	12.14%	9.89%	9.25%	8.23%	7.5%	7.11%	6.35%	6.35%	5.54%

6. Results and discussion

6.1. Simulation results

To verify the mathematical analysis, CHB-MLI was implemented and validated in Simulink/MATLAB to balance the output power of each stage. A 5-stage, 11-level inverter with SCM was considered to feed an impedance load with an active power of 300 W and reactive power ranging from 300 VAR capacitive to 500 VAR inductive as an independent load. The DC input of the inverter was 35VDC. A schematic diagram of the inverter and the measurement equipment is shown in Fig. 4. The output power of each inverter stage for different impedance loads is shown in Fig. 5. First, consider a 300 W, -300VAR resistive

capacitive load with $\varphi = +45°$. Fig. 5(a) shows the power of each stage with the three modulation methods (FIFO, FILO, and BPSCM). The power deviation of each stage with the variance index is presented in the table below each figure. As shown in Fig. 2, in the FILO method, the power of the first cell is greater than that of the last cell, regardless of whether φ is negative or positive, and this difference is maximized at φ=0. In the FIFO method, for RC loads or negative φ, the power of the first cell is greater than that of the last cell, as confirmed in Fig. 5(a). Finally, the BPSCM method exhibited almost uniform power for the RC load. For the RC load, the FILO method has less power deviation than FIFO, approximately 17.2 vs. 24.4, whereas the BPSCM method shows a variance of 1.9, that is, approximately 89% reduction. This indicates a significant improvement in balancing the power between the stages. Fig. 5(b) shows the results for a 300 W and +500VAR resistive inductive load with $\varphi = -59°$.

The FIFO method, which always generates more power in the first cell than in the last cell, yields the same results as those shown in Fig. 5(a). The situation is different for the FILO method in RL load; therefore, the power of the last cells is greater than that of the first cells. Again, for the RL load, the FILO method has a lower power deviation than the FIFO, approximately 16.5 vs. 38.9, whereas the BPSCM method shows a variance reduction of approximately 88%. This implies a significant reduction in the power imbalance between stages, and that the power between the stages is almost uniform. Fig. 5(c) shows the results for a net resistance load of 300 W. In this case, the FIFO method has a lower power deviation than FIFO, approximately 5.62 compared to 18.1. However, the BPSCM method exhibited a reduction of 66%, and the power of the stages was more uniform than that of the RC and RL loads. For all three types of impedance loads, the new algorithm showed a significant reduction in the power deviation between the stages. The THD is the same for all the three modulation methods because they produce the same output voltage waveform.

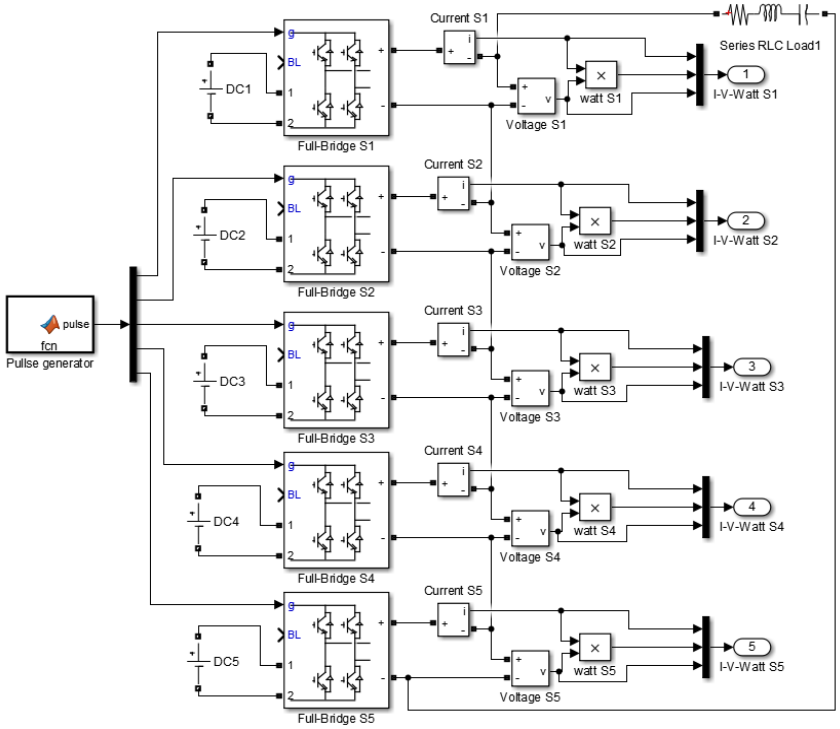

Fig. 4. Schematic diagram of 5-stage 11-level CHB-MLI connected to an RLC independent load in Simulink/MATLAB. Each stage is equipped with measurement devices to measure its output power, voltage and current. The MATLAB function sends the appropriate signals to each H-bridge module based on the different methods of FIFO, FILO, and BPSCM.

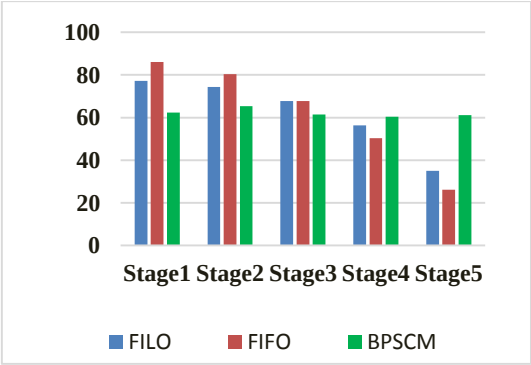

	FILO	FIFO	BPSCM
$\sigma^2(P)$	17.2	24.4	1.9
THD	8.01%	8.01%	8.01%

(a)

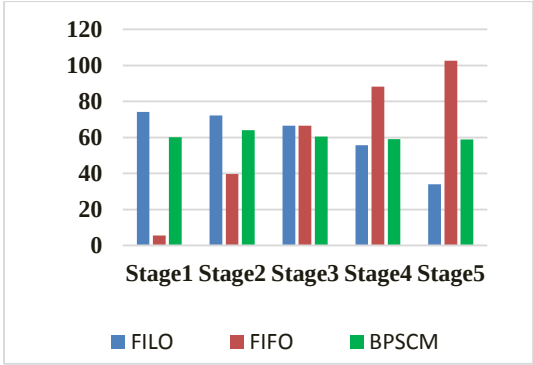

	FILO	FIFO	BPSCM
$\sigma^2(P)$	16.5	38.9	2.0
THD	8.1%	8.1%	8.1%

(b)

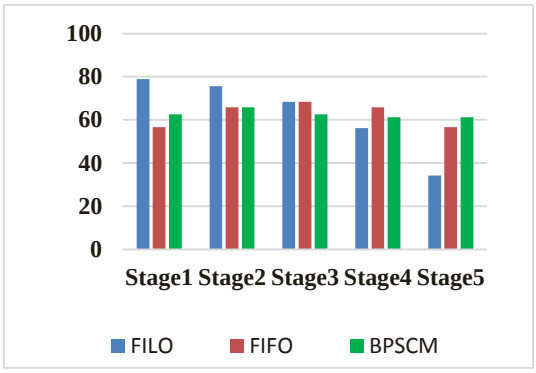

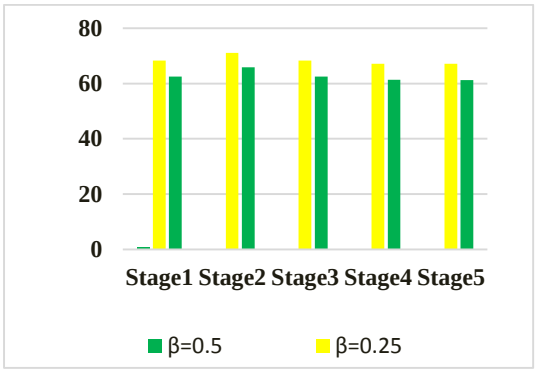

	FILO	FIFO	BPSCM
$\sigma^2(P)$	18.1	5.62	1.9
THD	8.23%	8.23%	8.23%

(c)

BPSCM	$\beta = 0.5$	$\beta = 0.25$
$\sigma^2(P)$	1.9	1.65
THD	8.23%	7.50%

(d)

Fig. 5. Individual power for each cell of a 5-stage CHB-MLI with SCM switching method. (a) for RC load with P=300W and Q=-300VAR or $\varphi = +45°$, (b) for RL load with P=300W and Q=500VAR or $\varphi = -59°$, (c) for a resistive load with P=300W, and (d) case (c) for two different value of β. The power deviation of stages and the THD of the output voltage for each modulation method is shown in the table below each chart.

According to Section 5.2, the efficiency can be increased again. If the turn-on angles of the first quarter by (4) are calculated for β=0.25 instead of 0.5, the variance of the power deviation will be even smaller. The results are shown by the two different β values in Fig. 5(d) for the net resistive load. In addition, to reduce the variance of the power imbalance between cells from 1.9 to 1.65, the power of each stage was increased from 62 W to 70 W, which means a 14% increase in efficiency with the same DC source per cell. As shown in Fig. 5(d), because β changes, the output voltage waveform and the THD also change. The voltage and current waveforms of each stages for the three methods are shown in Figs. 6(a)–6(f).

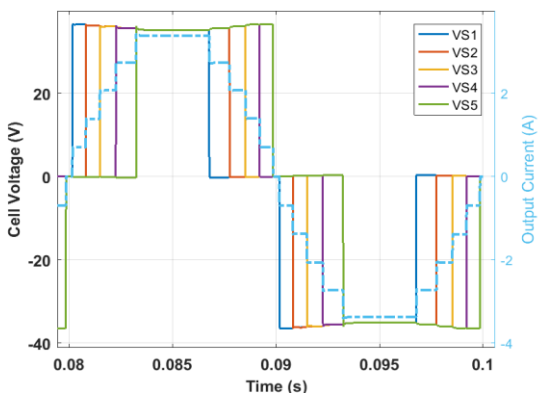

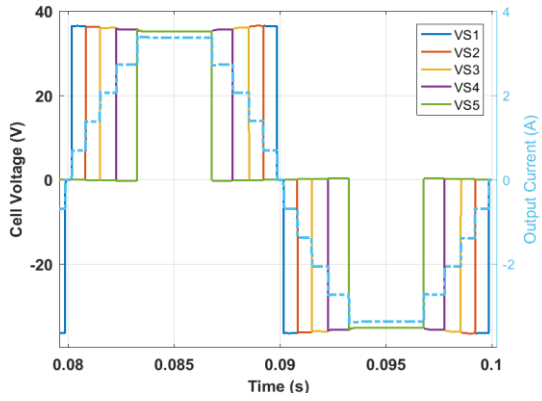

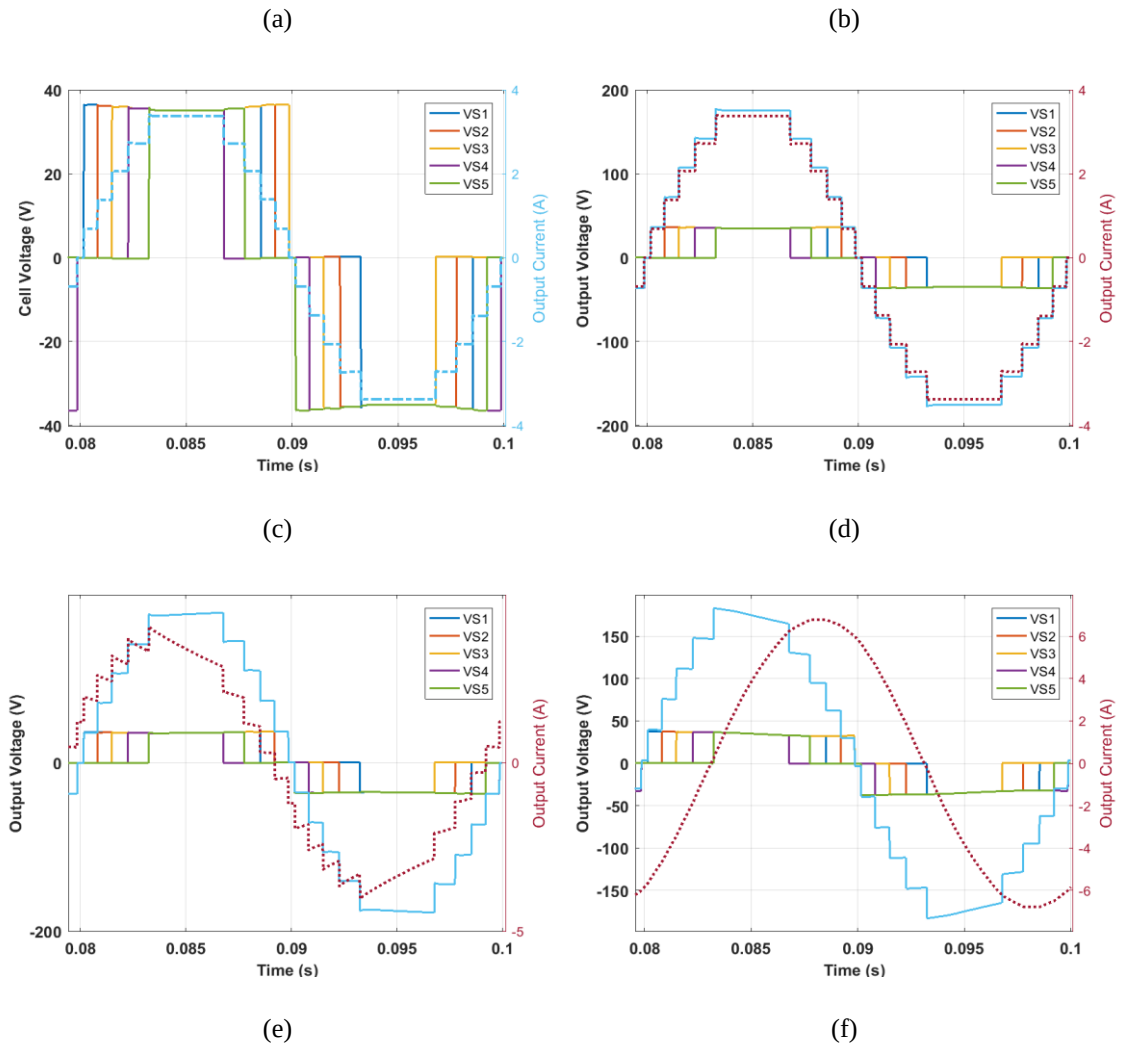

Fig. 6. Individual voltage waveforms for each cell of a 5-stage 11-level CHB-MLI with SCM switching methods. Voltage of stages for resistive load of 300W by (a) FIFO, (b) FILO, and (c) BPSCM. The output voltage and current waveforms of the entire inverter by BPSCM with (d) resistive load of 300W, (e) RC load of 300W and -300VAR, and (f) RL load of 300W and +500VAR.

Fig. 6(a) and 6(b) show the voltages across each inverter stage for the FIFO and FILO methods, respectively. Fig. 6(c) illustrates the voltage waveform of each cell using the BPSCM method. All three modulation methods produce an inverter output waveform, as shown in Fig. 6(d). In Figs. 6(a)–6(d), the load has a net resistance of 300 W. For further investigation, the voltage waveform of each stage along with the voltage waveform of the inverter output for RC loads of 300 W and -300VAR are depicted in Fig. 6(e). This is also repeated for RL loads of 300 W and +500VAR, as shown in Fig. 6(f).

6.2. Experimental results

Fig. 7 illustrates the experimental setup implemented in the laboratory to validate with experimental results the modulation method proposed in this study when applied to a 5-stage 11-level CHB-MLI.

The power plant runs in real time in an OPAL RT-4015 unit, which is programmed and monitored using the software OPAL RT-LAB. A dSPACE MicroLabBox compact prototyping unit was used to implement the modulation techniques of the system, and the dSPACE ControlDesk software allowed monitoring of the equipment. A Yokogawa DLM4038 oscilloscope was used to measure and represent the variables of interest in real time and to obtain the experimental results shown in the figures in this section.

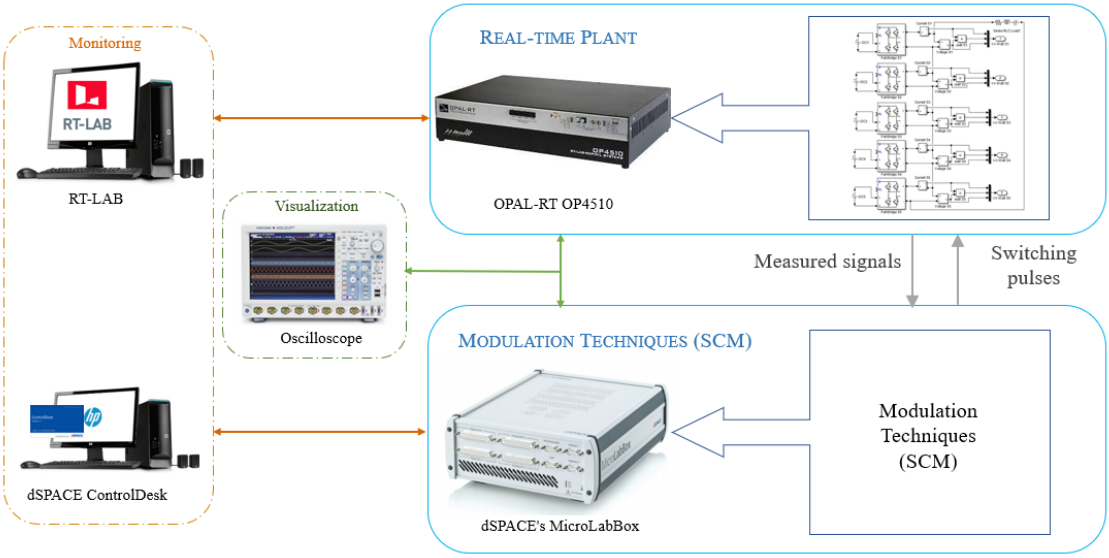

Fig. 7. Experimental setup implemented in laboratory. A 5-stage 11-level CHB-MLI runs in real-time in OPAL RT-4015 and the differents SCM are implemented in dSPACE MicroLabBox.

Fig. 8 shows the experimental results of the three modulation methods when the load was resistive-capacitive. The variables shown in the oscilloscope are the output power (PSi), output voltage (VSi), and current (ISi) of the i-th stage of the inverter. For example, PS1, VS1, and IS1 represent the power, voltage, and current of the first stage, respectively. Fig. 8(a) shows the output power, voltage, and current of stages 1 to 5 from top to bottom, and the last image shows the output voltage waveform of the inverter. As shown, it is consistent with the simulation results shown in Section 6.1, and the output powers of the stages in the BPSCM are closer to each other than the two methods.

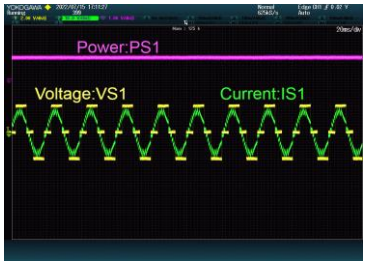

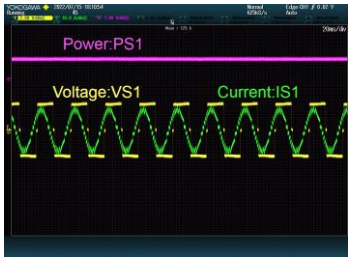

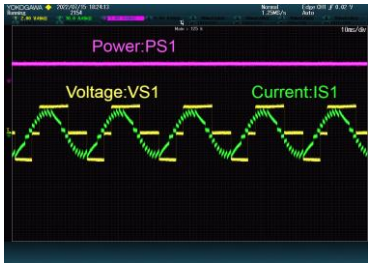

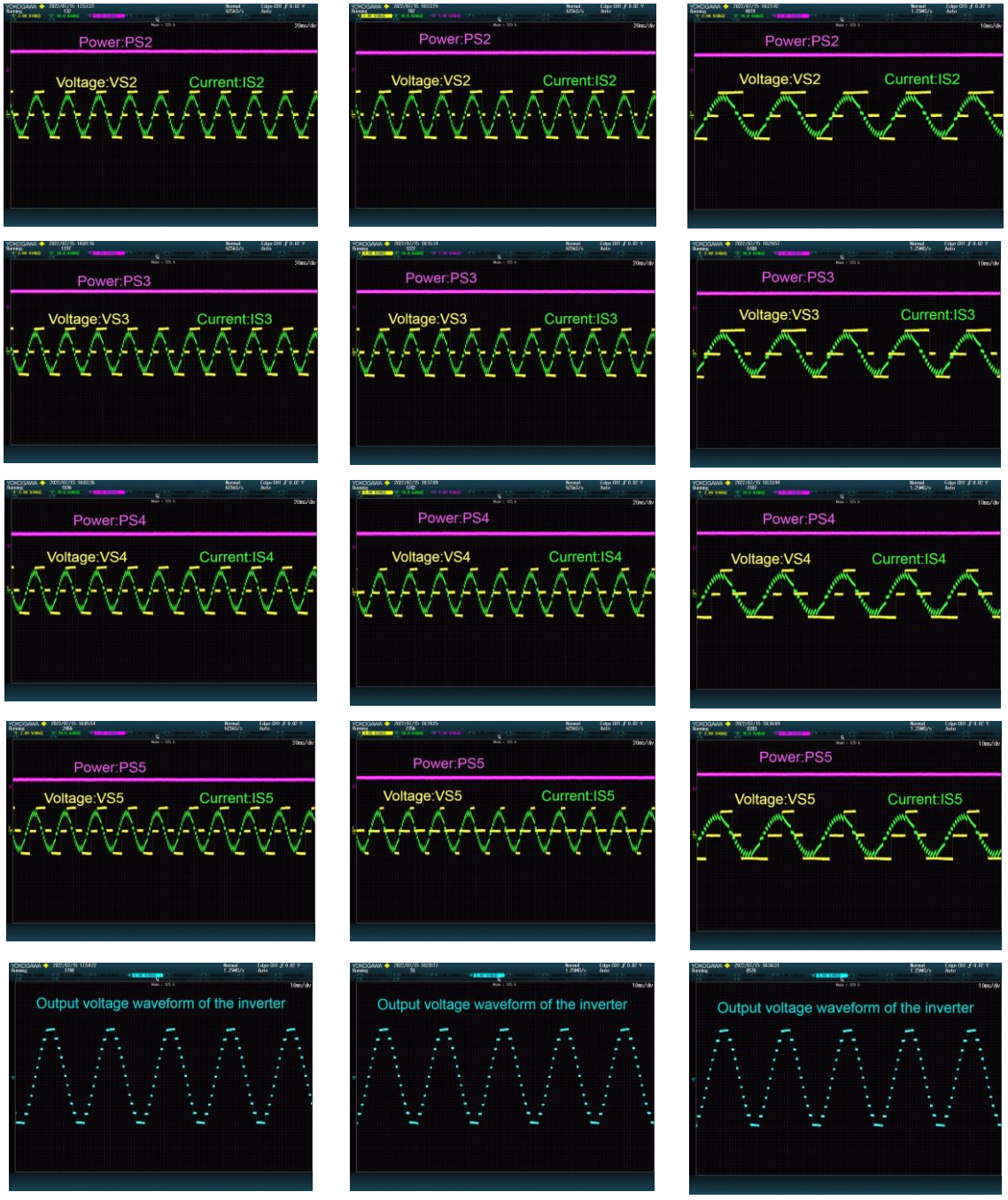

(a) (b) (c)

Fig. 8. Experimental results obtained for a 5-stage CHB-MLI with different SCM and RC load with P=300W and Q=-300VAR or $\varphi = +45°$ for (a) FIFO, (b) FILO, and (c) BPSCM.

Fig. 9, similar to Fig. 8, shows the experimental results for the three modulation methods when the load is resistive-inductive. For the FILO method, the power value of the last stage faces disturbances; for the BPSCM method, the experimental results are similar to the simulation results; and again, the power values of the stages in the new method are very close to each other, and the power deviation between the stages is very small.

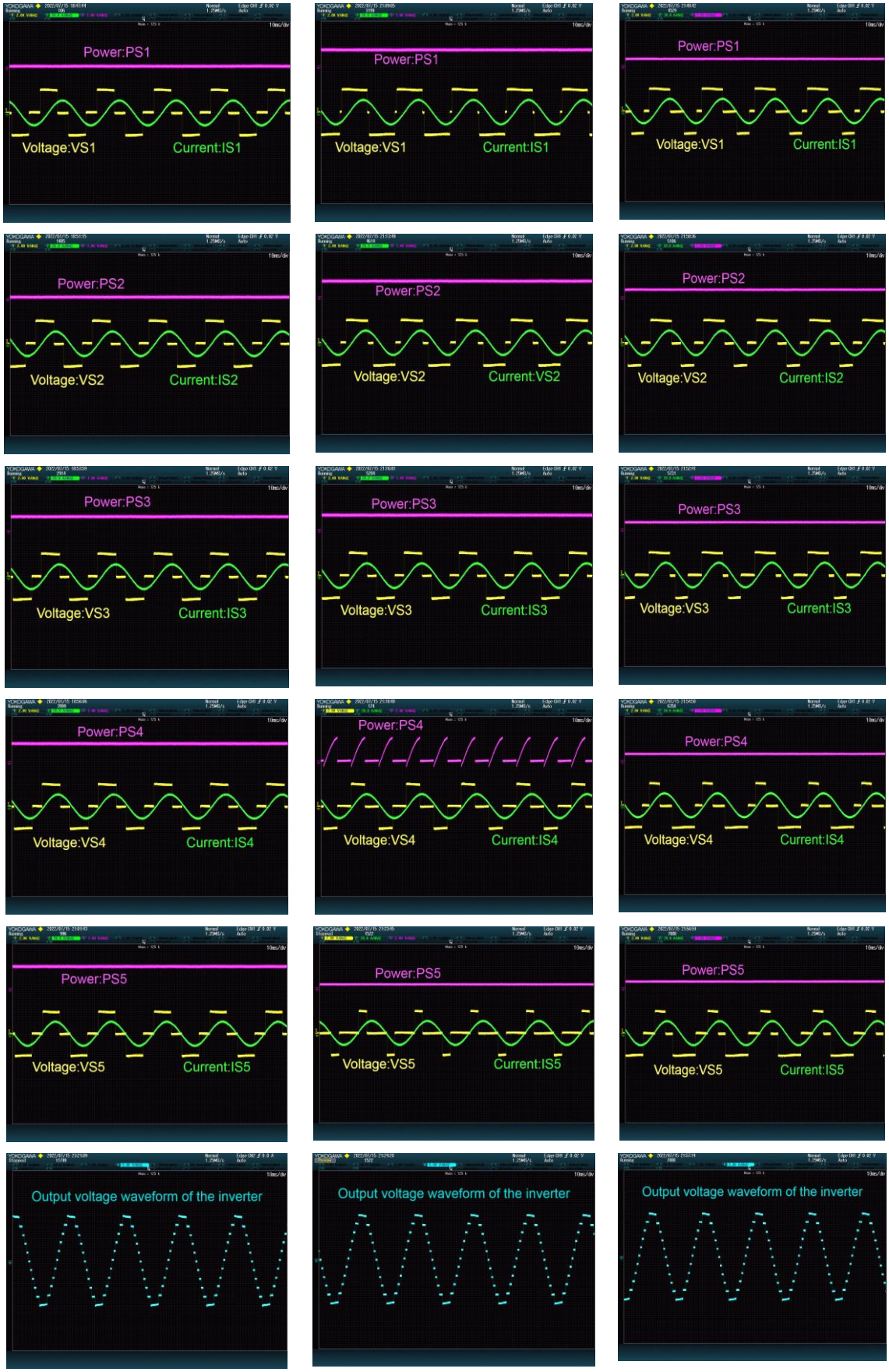
Power:PS1
Voltage:VS1
Current:IS1
Power:PS1
Voltage:VS1
Current:IS1
Power:PS1
Voltage:VS1
Current:IS1
Power:PS2
Voltage:VS2
Current:IS2
Power:PS2
Voltage:VS2
Current:VS2
Power:PS2
Voltage:VS2
Current:IS2
Power:PS3
Voltage:VS3
Current:IS3
Power:PS3
Voltage:VS3
Current:IS3
Power:PS3
Voltage:VS3
Current:IS3
Power:PS4
Voltage:VS4
Current:IS4
Power:PS4
Voltage:VS4
Current:IS4
Power:PS4
Voltage:VS4
Current:IS4
Power:PS5
Voltage:VS5
Current:IS5
Power:PS5
Voltage:VS5
Current:IS5
Power:PS5
Voltage:VS5
Current:IS5
Output voltage waveform of the inverter
Output voltage waveform of the inverter
Output voltage waveform of the inverter

(a) (b) (c)

Fig. 9. Experimental results obtained for a 5-stage CHB-MLI with different SCM and RL load with P=300W and Q=500VAR or $\varphi = -59°$ for (a) FIFO, (b) FILO, and (c) BPSCM.

Fig. 10 shows the experimental results for the three modulation methods with a purely resistive load, which is also consistent with the simulation results. Fig 10(c) shows that the power deviation between the stages is slightly greater than that in Figs. 8(c) and 9(c), which is confirmed by the analysis of the maximum power deviation that exists when the load angle is zero.

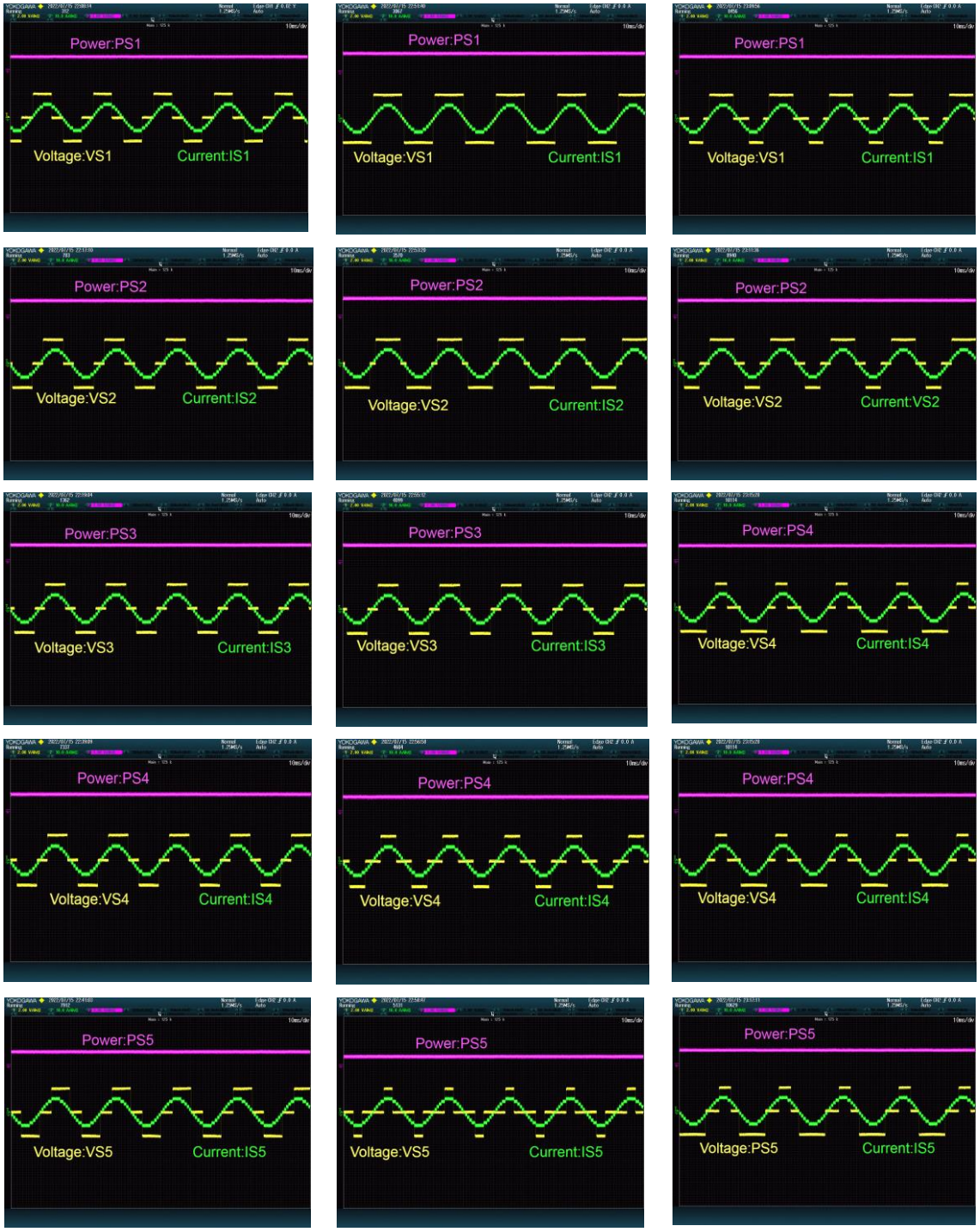

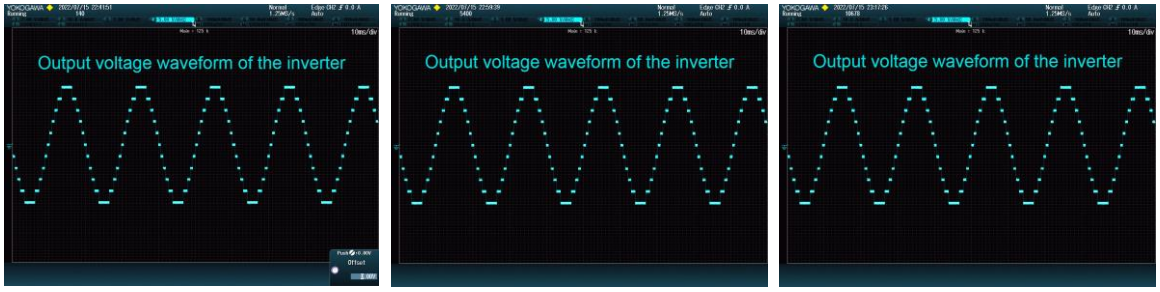

(a) (b) (c)

Fig. 10. Experimental results obtained for a 5-stage CHB-MLI with different SCM and resistive load of P=300W or $\varphi = 0°$ for (a) FIFO, (b) FILO, and (c) BPSCM.

6.3. Discussion

Both the experimental and simulation results of the mathematical analysis confirm the efficiency of the proposed method. The BPSCM method is preferable to the two common FILO and FIFO methods, both in terms of the THD and minimization of the power imbalance between stages. In addition, the BPSCM method is superior to the other methods published in the literature. In [28], the method was dependent on the load angle and was continuously re-calculted with it. Although it does not seem logical that the pattern changes continuously with the load angle, because the pattern solution itself is discrete and limited in number, and the NLC angles cannot be chosen at any arbitrary value. Every time the load angle changes, the calculations must be performed as a new one, and the complexity of these calculations is very time-consuming. The proposed method does not depend on the load angle, and the method is designed such that the power deviation is zero for a load angle of $\pm 90°$ and the deviation value is maximum only for $\varphi = 0°$, which is far less than the minimum power deviation of other methods used in the literature. Briefly, the advantages of the BPSCM are: 1) simple calculation, 2) the switching pattern is pre-determined by the number of stages, and 3) it is independent of the load angle.

7. Conclusion

High-frequency modulation methods, such as SPWM or low-frequency SCM, which are used for CHB-MLI operation, cannot distribute the power uniformly between the stages. In this study, a new algorithm based on SCM was designed for an optimum switching pattern. At first, a random vector with a sample space consisting of the random variables of the inverter stages power was stochastically analyzed. Subsequently, an optimization problem with finite and discrete solutions was defined on this random vector subject to power constraints for AC circuits. In fact, the solution to this random optimization

problem is the proposed algorithm. The mathematical analysis showed that the maximum power deviation between the stages occurs for zero load angle. Therefore, by focusing on minimizing the power deviation at a zero-load angle and zero power at pure impedance loads in each stage, a static algorithm similar to Sudoku puzzle was obtained that is not dependent on load angle. With this algorithm, by changing the impedance load angle, heavy calculations of the previous methods are not necessary. In addition, its practical implementation is simple. The simulation results obtained from the Simulink model and the experimental results obtained in the laboratory using OPAL RT-4510 and dSPACE MicroLabBox confirm the effectiveness of the proposed algorithm. In addition, the effect of the β coefficient, which changes the turn-on angles in the first quarter, was shown. By changing β, the angles of the first quarter change when compared to the angles obtained by the traditional NLC method. It can be proven that, for a certain β, the operational efficiency of the inverter increased significantly in terms of the output power and the reduction in the standard deviation of the power between stages.

Acknowledgements

This work was partially supported by the Regional Ministry of Economic Transformation, Industry, Knowledge, and Universities of Junta de Andalucía, under Grant PY20_00317.

References

[1] Liping Huang, Dashen Chen, Chun Sing Lai, Zhaoxiong Huang, Ahmed F. Zobaa, Loi Lei Lai. A Distributed Optimization Model for Mitigating Three-phase Power Imbalance with Electric Vehicles and Grid Battery. Electric Power Systems Research 2022; (210). doi:10.1016/j.epsr.2022.108080

[2] P. K. Chamarthi, A. Al-Durra, T. H. M. EL-Fouly and K. A. Jaafari. A Novel Three-Phase Transformer-less Cascaded Multilevel Inverter Topology for Grid-Connected Solar PV Applications. In IEEE Transactions on Industry Applications 2021;57(3), 2285-2297. doi: 10.1109/TIA.2021.3057312

[3] C. I. Odeh, A. Lewicki and M. Morawiec. A Single-Carrier-Based Pulse-Width Modulation Template for Cascaded H-Bridge Multilevel Inverters. In IEEE Access 2021, (9), 42182-42191. doi: 10.1109/ACCESS.2021.3065743

[4] V. Jain and R. Gupta. Digitization Effect in Implementation of Hybrid Modulation Technique in CHBMLI. IECON 2021 – 47th Annual Conference of the IEEE Industrial Electronics Society 2021; 1-6, doi:10.1109/IECON48115.2021.9589253.

[5] Vinothkumar, V., Kanimozhi, R. Power flow control and power quality analysis in power distribution system using UPQC based cascaded multi-level inverter with predictive phase dispersion modulation method. J Ambient Intell Human Comput **12,** 2021; 6445–6463. Doi:10.1007/s12652-020-02253-y

[6] C. I. Odeh, A. Lewicki and M. Morawiec, "A Single-Carrier-Based Pulse-Width Modulation Template for Cascaded H-Bridge Multilevel Inverters," in *IEEE Access*, vol. 9, pp. 42182-42191, 2021. doi:10.1109/ACCESS.2021.3065743.

[7] R. Sarker, A. Datta and S. Debnath. FPGA Implementation of Phase Disposition PWM (PD-PWM) Strategy for Cascaded H-Bridge Multilevel Inverter (CHB-MLI). IEEE Applied Signal Processing Conference (ASPCON) 2020; 80-84, doi: 10.1109/ASPCON49795.2020.9276676.

[8] Q. Cheng and C. Wang. Comparison of Phase-Shifted Carrier PWM Schemes for Modular Multilevel Converter. IEEE Energy Conversion Congress and Exposition (ECCE) 2019; 4801-4807, doi: 10.1109/ECCE.2019.8912558.

[9] E. Barbie, R. Rabinovici and A. Kuperman. Closed-Form Analytic Expression of Total Harmonic Distortion in Single-Phase Multilevel Inverters With Staircase Modulation. In IEEE Transactions on Industrial Electronics 2019; 67(6), 5213-5216, doi: 10.1109/TIE.2019.2922934.

[10] P. Mishra and A. Mahesh. Sine cosine algorithm-based staircase modulation for cascaded H-bridge inverter. 3rd International conference on Electronics, Communication and Aerospace Technology (ICECA) 2019; 914-919, doi: 10.1109/ICECA.2019.8822115.

[11] A. Sedaghati, H. Sánchez, L. M. Ramirez. Comparative Study of the Suitable Modulation Methods for Cascade H-Bridge Multi-Level Inverter. ICEEE 2021- International Conference on Electrcial and Electronic Engineering 2021; 1-6. https://worldresearchlibrary.org/proceeding.php?pid=4499.

[12] V. K. Sharma, M. Kumar, K. K. Gupta and M. Kirar. Power balancing in five level inverters. 12th International Conference on Environment and Electrical Engineering 2013; 434-439. doi:10.1109/EEEIC.2013.6549555.

[13] Gong, R., Zhang, X., Liu, J., Xue, B. A new modulation strategy and power balance method of unsymmetrical CHB inverter. IET Renew. Power Gener. 2021; 00, 1-10.

[14] Y. Wang, K. Wang, G. Li, F. Wu, K. Wang and J. Liang. Generalized Switched-Capacitor Step-up Multilevel Inverter Employing Single DC Source. In CSEE Journal of Power and Energy Systems, 2022; 8(2), 439-451, March 2022. doi:10.17775/CSEEJPES.2020.06280.

[15] C. I. Odeh, A. Lewicki, and M. Morawiec. A single-carrier-based pulse-width modulation template for cascaded H-bridge multilevel inverters. IEEE Access, 2021; 9, 42182-42191.

[16] M. Ye, R. Peng, Z. Tong, Z. Chen and Z. Miao. A Generalized Scheme With Linear Power Balance and Uniform Switching Loss for Asymmetric Cascaded H-Bridge Multilevel Inverters. In IEEE Transactions on Power Electronics, 2022; 37(3), 2719-2730. doi:10.1109/TPEL.2021.3114369.

[17] Carrara G., Gardella S., Marchesoni M. A new multilevel PWM method: a theoretical analysis. IEEE Trans. Power Electron 1992; 7, 497–505.

[18] Hammond P.W. A new approach to enhance power quality for medium voltage drives. 42nd Annual Petroleum and Chemical Industry Conf., 1995. Industry Applications Society. IEEE 1995; 231–235.

[19] J. Li. et al. DC Voltage Utilization Improvement to Enlarge Power Balance Constraint Range for Photovoltaic Cascaded Inverter. IEEE Access 2021; 9, 123603-123615. doi:10.1109/ACCESS.2021.3072852.

[20] M. Miranbeigi and H. Iman-Eini. Hybrid modulation technique for grid-connected cascaded photovoltaic systems. IEEE Trans. Ind. Electron 2016; 63(12), 7843-7853.

[21] M. Wang et al. Module Power Balance Control Strategy for Three-Phase Cascaded H-Bridge PV Inverter Under Unbalanced Grid Voltage Condition. In IEEE Journal of Emerging and Selected Topics in Power Electronics 2021; 9(5), 5657-5671. doi:10.1109/JESTPE.2021.3063524.

[22] S. Kouro, C. Fuentes, M. Perez, and J. Rodriguez. Single DC-link cascaded H-bridge multilevel multistring photovoltaic energy conversion system with inherent balanced operation. In Proc. 38th Annu. Conf. IEEE Ind. Electron. Soc. (IECON), Montreal, QC, Canada, Oct. 2012; 4998–5005.

[23] Uthen Kamnarn, Viboon Chunkag. Power balance control technique of the modular three-phase ac to dc converter with fast transient response. Electric Power Systems Research, 2007; 77(12), 1585-1594, ISSN 0378-7796, doi:10.1016/j.epsr.2006.11.005.

[24] Ye, M., Kang, L., Xiao, Y., Song, P. and Li, S. Modified hybrid modulation strategy with power balance control for H-bridge hybrid cascaded seven-level inverter. IET Power Electronics 2018; 11, 1046-1054. doi:10.1049/iet-pel.2017.0558

[25] Manjrekar, M., Steimer, P., Lipo, T. Hybrid multilevel power conversion system: a competitive solution for high-power applications. IEEE Trans. Ind. Appl. 2000; 36(3), 834–841.

[26] M. Ye, W. Ren, L. Chen, Q. Wei, G. Song and S. Li. Research on Power-Balance Control Strategy of CHB Multilevel Inverter Based on TPWM. In IEEE Access 2019; 7, 157226-157240. doi:10.1109/ACCESS.2019.2950064

[27] O. Lopez-Santos, C. A. Jacanamejoy-Jamioy, D. F. Salazar-D'Antonio, J. R. Corredor-Ramírez, G. Garcia and L. Martinez-Salamero. A Single-Phase Transformer-Based Cascaded Asymmetric Multilevel Inverter With Balanced Power Distribution. In IEEE Access 2019; 7, 98182-98196. doi:10.1109/ACCESS.2019.2930230

[28] L. M. Kunzler and L. A. C. Lopes. Algorithm for Improving Power Balance for Cascaded H-Bridge Multilevel under Staircase Modulation for Linear Loads. IECON 2019; 45th Annual Conference of the IEEE Industrial Electronics Society, pp. 6066-6071. doi:10.1109/IECON.2019.8927489

[29] P. M. Meshram and V. B. Borghate. A simplified nearest level control (NLC) voltage balancing method for modular multilevel converter (MMC). IEEE Transactions on Power Electronics 2015; 30(1), 450-462.

[30] B. He, K. Ma, X. Xin and W. Wang. Hybrid Modulation Method for Nearest-Level-Control-Based MMC to Suppress DC Power Fluctuation When Enabling Circulating Current Suppression. IEEE Energy Conversion Congress and Exposition (ECCE), 2020, 6232-6237, doi: 10.1109/ECCE44975.2020.9235357.

Conflict of Interest

Declaration of interests

■ The authors declare that they have no known competing financial interests or personal relationships that could have appeared to influence the work reported in this paper.

☐The authors declare the following financial interests/personal relationships which may be considered as potential competing interests:

CRediT authorship contribution statement

Alireza Sedaghati: Conceptualization, Formal analysis, Investigation, Methodology, Software, Validation, Visualization, Writing - original draft, Writing - review & editing.

Pablo Horrillo-Quintero: Methodology, Software, Investigation, Validation, Visualization, Writing - review & editing.

Higinio Sánchez-Sainz: Conceptualization, Formal analysis, Methodology, Writing - review & editing.

Luis M. Fernández-Ramírez: Conceptualization, Funding acquisition, Methodology, Project administration, Supervision, Investigation, Writing - review & editing.